Ceramics

Rapid fabrication of Ga-doped Li$_7$La$_3$Zr$_2$O$_{12}$ powder via microwave-assisted solution combustion synthesis

Christopher S. Dandeneau[1,*] , Rahul Rajeev[2], Kyle S. Brinkman[2] , Dale A. Hitchcock[1] , and Brenda L. Garcia-Diaz[1]

[1] *Savannah River National Laboratory, Aiken, SC 29803, USA*
[2] *Department of Materials Science and Engineering, Clemson University, Clemson, SC 29634, USA*

ABSTRACT

Garnet-type Li$_7$La$_3$Zr$_2$O$_{12}$ (LLZO) ceramics have been explored as solid-state electrolytes for energy conversion and storage applications. However, high Li volatility makes LLZO fabrication by conventional solid-state routes challenging. Here, a microwave-assisted solution combustion synthesis (SCS) process was developed to produce undoped and Ga-doped LLZO powders. Effects of two fuels, urea and glycine, on the kinetics of undoped LLZO SCS reactions were evaluated by IR camera imaging; peak temperatures were compared with adiabatic temperatures (T_{ad}) from thermodynamic calculations. When compared to glycine, urea was found to be a more suitable fuel for ensuring complete combustion and inducing a higher degree of crystallinity in the as-processed powder. Such a finding could possibly be attributed to the formation of more thermodynamically stable metal-glycine complexes, which lowers the reducing power of the fuel and decreases reaction exothermicity. X-ray diffraction analysis of powder fabricated with urea as the fuel showed that heat from the SCS reaction alone was sufficient to crystallize ∼80% of the precursor into tetragonal LLZO; full crystallization was achieved after calcination at 950 °C for 5 h. Urea was subsequently employed to produce Ga-doped LLZO via SCS. As-processed powder was nearly 60% cubic LLZO; full crystallization was achieved upon calcination. Optimization of SCS reaction chemistry may enable synthesis of single-phase cubic LLZO without the need for a calcination step, greatly simplifying the LLZO fabrication process.

Introduction

Current efforts to mitigate fossil fuel dependency and enable more widespread adoption of sustainable energy sources have spurred the development of new materials and processing technologies. Such trends are readily apparent in the field of Li-ion battery (LIB) research, where there has been a continued push to find replacements for liquid organic electrolytes due to issues related to safety and compatibility [1–3]. The fluidic nature of liquid electrolytes and the need for separators also impose constraints that limit the range of device configurations [4]. To expand the applicability of LIBs and enable their use on a larger scale, recent studies have focused on inorganic solid-state Li-ion conductors as alternatives to conventional liquid-based electrolytes [5–10]. In particular, solid oxide electrolytes possess material properties that are well-suited for implementation in energy storage and conversion systems, including good thermal and chemical stability, high mechanical strength, relatively high ionic conductivity, and the capability for miniaturization via thin film processing methods [11–16].

Among the candidate oxides explored as solid-state electrolytes, garnet-type $Li_7La_3Zr_2O_{12}$ (LLZO) ceramics have been extensively investigated due to their good Li-ion conductivity ($\sim 10^{-3}$ S cm^{-1} in the cubic phase), high chemical stability toward elemental Li, and wide window of electrochemical stability [17–21]. In addition to the aforementioned energy and conversion applications, LLZO has been studied as a candidate solid Li-ion conductor for the separation of tritium from Li in fusion applications [22]. The ionic conductivity of tetragonal LLZO, the stable polymorph at room temperature, is approximately two orders of magnitude lower than that of cubic LLZO. Consequently, substantial efforts have been devoted to the stabilization of cubic phase LLZO at room temperature. Both computational and experimental studies have demonstrated that substitutional doping on the Li- and/or Zr sublattice by supervalent cations (e.g., Al^{3+} [23–25], Ga [26, 27] for Li and/or Nb [28], Ta [29, 30] for Zr) serves to stabilize cubic LLZO by increasing the concentration of Li vacancies formed to preserve lattice electroneutrality. However, the fabrication of doped cubic LLZO is challenging, as the conductivity is dependent upon control of overall material stoichiometry,

and suppressing Li loss due to volatilization during repeated high-temperature calcination (to induce crystallization) and sintering steps is a formidable task [31, 32].

Conventional solid-state reaction (SSR) synthesis is the most common method for fabricating LLZO due to its low cost, relative simplicity, and capacity for high throughput when compared to other processing techniques. In a typical SSR procedure for cubic LLZO, solid cationic precursors are milled to ensure thorough mixing and reduce particle size, and then calcined at high temperature (usually > 900 °C). This process of milling and calcination is then repeated until a powder with sufficiently high phase purity is produced. The as-fabricated cubic LLZO can ultimately be pressed into a green body and sintered at higher temperatures typically (1000 to 1200 °C) to yield a dense ceramic [18]. Despite the advantages of the SSR technique, the limited intermixing of solid precursors during mechanical milling means that atoms must diffuse over larger distances for crystallization and densification. This in turn requires higher temperatures and/or longer heating times, which increases the extent of Li loss [33]. While certain measures can be implemented to mitigate Li loss (e.g., addition of excess Li precursor, covering pellets in mother powder during sintering), Li vaporization associated with repeated milling/calcination treatments and sintering at higher temperatures/longer times decreases processing efficiency and makes strict control of LLZO stoichiometry more difficult.

Wet chemistry techniques have been developed as alternatives to SSR routes, and cubic LLZO has been successfully produced via the Pechini method [34], sol-gel processing [35], co-precipitation [11], and solution combustion synthesis (SCS) [36, 37]; molten salt synthesis of LLZO has also been explored [38]. (Note: Wet chemistry is used here to refer to powder synthesis and not the wet-processing of calcined LLZO slurries, where protic solvents such as water may have deleterious effects on the crystal structure and Li-ion conductivity [39].) One benefit of solution-based methods is the intermixing of LLZO cations on the molecular level, which can potentially decrease processing temperatures and reduce Li loss. Wet chemical routes also provide the capability to produce nano-sized LLZO powders with high sinterability. Among the above-mentioned synthesis techniques, SCS can provide particular advantages, including: 1) the use of water-soluble metal nitrate

oxidizers and reducing agents (i.e., fuels) in the combustion reaction, which simplifies the fabrication process by eliminating the need for organic solvents and strong chelating agents, 2) ease of scalability and potential for high-throughput, and 3) use of microwave irradiation to initiate the desired combustion reaction, which improves processing efficiency and reduces energy input, and 4) the ability to achieve partial or full crystallization rapidly using heat from the designed exothermic reaction, thereby reducing calcination temperature/time (or potentially eliminating the need for calcination with optimized reaction parameters) and mitigating Li loss.

In this work, undoped and Ga-doped LLZO powders were fabricated by a microwave-assisted SCS route. Temperature profiles of SCS reactions conducted with two different fuels, glycine and urea, were recorded with an IR camera. X-ray diffraction (XRD) analysis of as-combusted powders revealed that more complete combustion occurred with urea as the fuel. In the case of Ga-doped LLZO, appreciable crystallization of the cubic LLZO structure was achieved from energy released in the SCS reaction, and single-phase LLZO was produced after calcination at 950 °C for 5 h. To the best of our knowledge, no reports have yet been published on the fabrication of cubic LLZO via microwave-assisted SCS. The results presented in this work may open up a pathway for the processing of cubic LLZO powder in a rapid, single-step process at lower temperatures.

Materials and methods

Anhydrous $LiNO_3$, $La(NO_3)_3 \cdot 6H_2O$, $ZrO(NO_3)_2\text{-}xH_2O$, and $Ga(NO_3)_3 \cdot xH_2O$ were procured from Sigma-Aldrich for use as cation-bearing oxidizers. The $LiNO_3$ was transferred to an inert glovebox for storage upon receipt, while thermogravimetric analysis (TGA) was conducted on representative samples of the remaining metallic nitrates to ascertain waters of hydration. Urea and glycine (Sigma-Aldrich) were employed as fuels (i.e., reducing agents) and utilized as-received. Aqueous nitrate precursor solutions were prepared with cation molar ratios of 7.7:3:2 (Li:La:Zr) and 6.05:0.5:3:2 (Li:Ga:La:Zr) for $Li_7La_3Zr_2O_{12}$ (undoped LLZO) and $Li_{5.5}Ga_{0.5}La_3Zr_2O_{12}$ (Ga0.5-LLZO) target compositions, respectively; it was determined that 10 mol% excess Li content was necessary to compensate for Li loss and ensure phase

purity of the final product. For undoped LLZO, $LiNO_3$ was first weighed out in an inert glovebox, removed to ambient atmosphere, and dissolved in a minimum amount of deionized (DI) water under stirring at 85 °C on a hot plate for 30 min. A separate aqueous La/Zr nitrate solution was prepared by the sequential dissolution of $ZrO(NO_3)_2$ and $La(NO_3)_3$ in DI water under stirring on a hot plate at 85 °C for 1 h. The concentration of fuel for the aqueous solutions was determined such that the elemental stoichiometric coefficient ($\phi_e = O/R$, where O and R are the sum of the valences of the oxidizing and reducing components in the reactants) of the SCS reactions was unity when neglecting the excess Li addition [40]. Upon the addition of fuel to the Li and La/Zr nitrate mixtures, the solutions were stirred at 85 °C for 30 min and then combined into a single SCS precursor. This combined solution was stirred for an additional 30 min prior to microwave irradiation. Ga0.5-LLZO precursors were prepared in a similar manner with the addition of $Ga(NO_3)_3$ to the La/Zr nitrate solution.

To initiate the desired exothermic combustion reactions, approximately 20 mL of SCS precursor solution was pipetted into a quartz vial. Quartz was utilized due to its excellent thermal shock resistance when compared to that of other glass compositions. While the use of borosilicate glass did not have any deleterious effects on the as-processed powder during initial experiments, cracking and fracture of the vials upon cooling motivated the use of quartz. Heating of the SCS precursors was conducted with a single-mode CEM Discover microwave reactor operating at a power of 300 W and frequency of 2.45 GHz. Following irradiation of the solutions and initiation of an SCS reaction, vessels were allowed to cool naturally to room temperature (cooling time < 10 min). Temperatures of the solutions throughout the SCS process were recorded using a FLIR SC645 IR camera mounted above the microwave reactor cavity. The camera has a temperature accuracy of 2% over a range of −20 °C to 2000 °C, focal length of 24.6 mm, spectral range of 7.5–14 μm, and 0.69 mrad of spatial resolution.
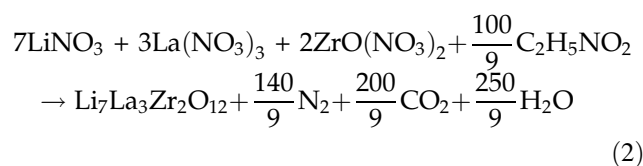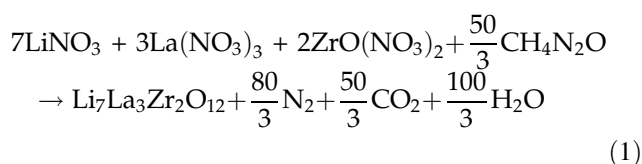
As-processed powder samples were loaded into a 12.7 mm stainless steel die and isostatically cold-pressed at a pressure of 150 MPa for 1 min. Pressed pellets were loaded into a Pt crucible, placed on a bed of mother powder, and then covered in as-processed mother powder to minimize Li loss during heating.

Use of Al_2O_3 crucibles was avoided so as to eliminate Li-Al reactions and prevent unintentional doping of the LLZO with Al [41, 42]. The crucibles were subsequently covered with a Pt lid, inserted into an alumina tube furnace, and calcined in air at 950 °C for 5 h; the heating rate was 5 °C min^{-1}. At the conclusion of the heat treatment, calcined powders were transported to an inert glovebox prior to further analysis.

The crystal structure of as-processed and calcined specimens was analyzed from XRD data acquired with a Rigaku instrument using Cu Kα ($\lambda = 1.5406$ Å) radiation; the scan rate was 1° min^{-1}. Rietveld refinement of the XRD patterns was carried out with SmartLab Studio II (Rigaku) software. Powder morphology was evaluated by scanning electron microscopy (SEM) images obtained with a Hitachi SU5000 variable pressure SEM operated with an accelerating voltage of 20 kV. The composition of the powders was determined by inductively-coupled plasma optical emission spectrometry (ICP-OES); specimens for analysis were prepared by sodium peroxide fusion. ICP data were collected in duplicate, and stoichiometry was calculated by normalization of the results to 3.00 moles of La. Oxygen content was ascertained by charge balance such that electroneutrality in the LLZO lattice is preserved.

Results and discussion

To induce phase formation during the SCS process and reduce the time/temperature needed for calcination of as-combusted powders, reactions were conducted with the goal of maximizing exothermicity and achieving complete combustion with little to no carbonaceous residue. In other words, the aim was to design an SCS reaction that reached higher temperatures over a longer time duration. It should be noted that "longer time" at higher temperatures, as it pertains to SCS reactions, is typically on the order of less than one minute. In this work, two commonly used SCS fuels, urea and glycine, were chosen for the synthesis of undoped LLZO; the SCS reactions with urea [Reaction (1)] or glycine [Reaction (2)] as the fuel can be expressed as:

$$7LiNO_3 + 3La(NO_3)_3 + 2ZrO(NO_3)_2 + \frac{50}{3}CH_4N_2O$$
$$\rightarrow Li_7La_3Zr_2O_{12} + \frac{80}{3}N_2 + \frac{50}{3}CO_2 + \frac{100}{3}H_2O \quad (1)$$

$$7LiNO_3 + 3La(NO_3)_3 + 2ZrO(NO_3)_2 + \frac{100}{9}C_2H_5NO_2$$
$$\rightarrow Li_7La_3Zr_2O_{12} + \frac{140}{9}N_2 + \frac{200}{9}CO_2 + \frac{250}{9}H_2O \quad (2)$$

For a theoretical comparison of the effect of fuel type on SCS reaction thermodynamics, the adiabatic temperature (T_{ad}) was calculated for Reactions (1) and (2). This parameter represents the maximum attainable temperature if all energy released during the exothermic reaction is utilized to heat the product materials; it can be derived from the following expression [43]:

$$\Delta Hr° = \int_{298}^{T_{ad}} \sum n_i C_{p,i} \quad (3)$$

where $\Delta H_r°$ is the standard enthalpy of the reaction at 298 K, while n_i and $C_{p,i}$ are, respectively, the moles and heat capacity of the ith product. Using the enthalpy of formation ($\Delta H_f°$) and heat capacity data shown in Table 1 [44–47], T_{ad} values for Reactions 1 and 2 were calculated to be 1371 °C ($\Delta H_r°$ = -4952.5 kJ) and 1618 °C ($\Delta H_r°$ = −5482.5 kJ), respectively. In reality, temperatures reached during SCS are lower due to factors such as heat loss by radiative transfer and incomplete combustion [48].

Shown in Fig. 1a are the temperature-time profiles recorded with an IR camera for microwave SCS reactions carried out with urea (U) and glycine (G); associated still images from IR video captured at different times during the reactions are displayed in Fig. 1b. In contrast to the theoretical T_{ad} values calculated above, much higher reaction temperatures were observed with urea (maximum of $\sim$1293 °C) when compared to glycine (maximum of $\sim$472 °C). Furthermore, the glycine reaction exhibited a much faster cooling rate after reaching maximum temperature. Inspection of the samples upon cooling revealed that incomplete combustion occurred for the solution with glycine, as the powder was brownish in color as opposed to fluffy and white as in the case of urea. This is supported by XRD data in Fig. 2a, where the sample made with urea shows prominent peaks from tetragonal LLZO as well as $La_2Zr_2O_7$ pyrochlore and La_2O_3 phases, while only peaks from $La_2Zr_2O_7$ are visible for the powder fabricated with glycine. Upon calcination at 950 °C for 5 h, the powder made with urea is transformed to single phase tetragonal

LLZO, as displayed in Fig. 2b. Applying the same calcination treatment to the glycine sample induced the formation of some tetragonal LLZO, but high-intensity peaks from $La_2Zr_2O_7$ along with reflections from La_2O_3 are still visible. Rietveld analysis was employed to quantify phase percentages and unit cell parameters; the results are presented in Table 2. The obtained XRD patterns and IR temperature data suggest a greater degree of overall energy release in the SCS reaction with urea as the fuel, which in turn led to the formation and partial crystallization of tetragonal LLZO.

Table 1 Thermodynamic values used to calculate T_{ad} for microwave SCS reactions

Substance	ΔH_f° (kJ/mol)		
$LiNO_3$	-483.1[a]		
$La(NO_3)_3$	-1329.3[a]		
$ZrO(NO_3)_2$	-1948.6[b]		
CH_4N_2O	-333.1[a]	$C_p = A + BT$ (kJ/mol·K)	
$C_2H_5NO_2$	-527.8[a]	A	B
N_2	0	0.0328[d]	5.93E-7[d]
CO_2	-393.5[a]	0.0546[d]	1.05E-6[d]
H_2O	-241.8[a]	0.0347[d]	1.45E-6[d]
$Li_7La_3Zr_2O_{12}$	-7152.6[c]	0.5337[c]	1.28E-4[c]
[a] = Ref. [44], [b] = Ref. [45], [c] = Ref. [46], [d] = Ref. [47]			

Displayed in Fig. 3 are SEM images acquired for undoped LLZO when urea is utilized as the fuel in the microwave SCS reaction. For the as-processed powder in Fig. 3a, ultrafine nanoscale particles are observed along with larger, almost micron-sized particles. The ability to produce ultrafine (i.e., < 100 nm) oxide powders by SCS has been well-documented and can be attributed to short processing times and the evolution of a large volume of gaseous products during the reaction [49–52]. Referring to Fig. 1 when urea was employed as the fuel, rapid heating to a temperature of nearly 1300 °C serves to crystallize ∼80% of the material into tetragonal LLZO. At the same time, gas evolution during the reaction allows for heat dissipation, which in turn inhibits particle growth. However, as evident in Fig. 3a, some degree of pre-sintering among particles did indeed occur, giving rise to fraction of larger particles with sizes that appear to be on the order of 100s of nanometers to a few microns. Upon calcination of the powder, most of the ultrafine particles, which possess a higher surface area and a larger driving force for sintering, coalesce into larger particles, as shown in Fig. 3b.

There are few possible scenarios to explain the findings observed with the different fuel types. Firstly, the T_{ad} calculations do not consider complexation of metal cations by the fuel. Although the formation of these complexes aids in dissolution of the metal nitrates, the stability of the metal complex
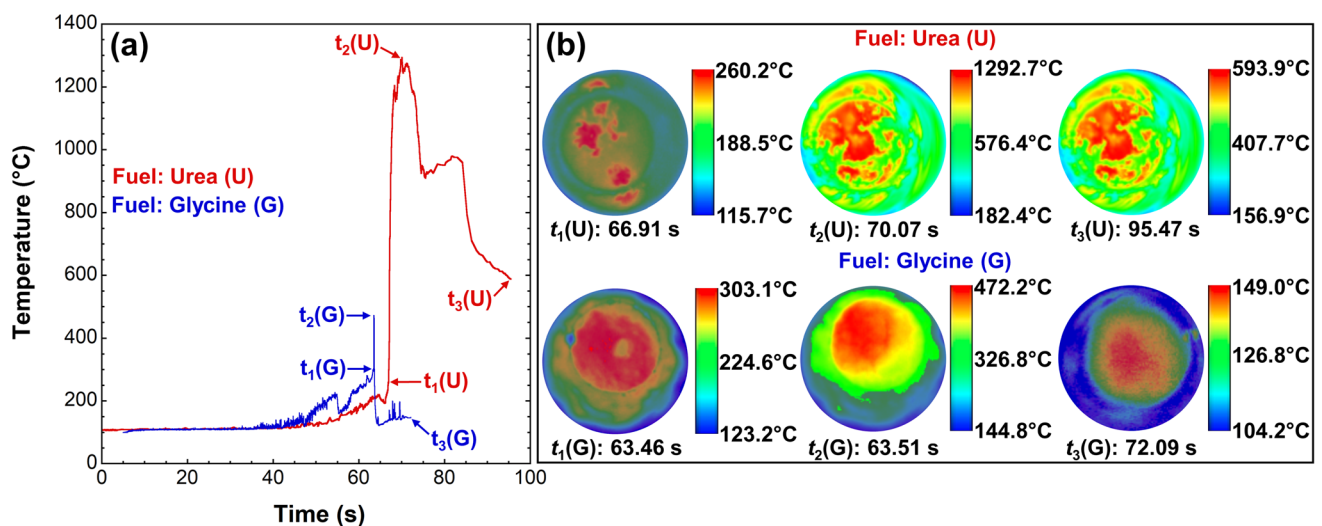

Figure 1 a Temperature profiles recorded with an IR camera during microwave-assisted SCS of undoped LLZO with glycine (G) and urea (U); **b** images captured for reactions with urea (top) and glycine (bottom) at the point of ignition (t_1), peak temperature (t_2), and removal of microwave irradiation (t_3).
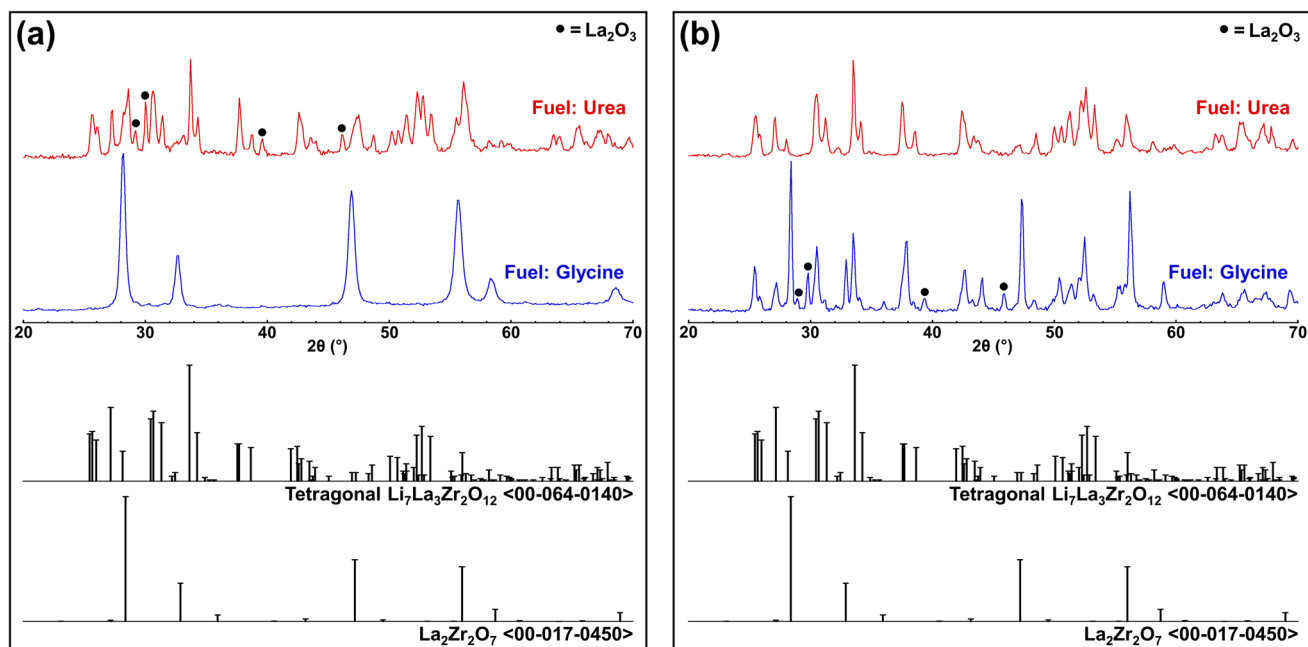
Figure 2 XRD patterns obtained for (**a**) as-processed and (**b**) calcined (950 °C/5 h) undoped LLZO fabricated with urea or glycine as the fuel; reference patterns for $La_2Zr_2O_7$ and tetragonal $Li_7La_3Zr_2O_{12}$ are also shown.

should not be so high that it hinders the reducing powder of the fuel [53]. Glycine is known to chelate metals with bidentate coordination, while urea typically coordinates as a monodentate ligand [54, 55]. In this work, solutions made with glycine and $ZrO(NO_3)_2$ went from milky white to transparent significantly faster (< 5 min) than with those prepared with urea (~30 min), an indicator of more effective complexation with glycine. Considering the data obtained for undoped LLZO, urea was chosen as the fuel to fabricate Ga0.5-LLZO via microwave-assisted SCS.

The XRD patterns of as-processed and calcined Ga0.5-LLZO are shown in Fig. 4. Prominent peaks

from cubic LLZO appear along with peaks from $La_2Zr_2O_7$ pyrochlore and La_2O_3. Rietveld refinement revealed the percentages of cubic LLZO, $La_2Zr_2O_3$, and La_2O_3 to be 59.9, 26.1, and 14.0, respectively. A subsequent calcination treatment at 950 °C for 5 h was sufficient for full crystallization of the powder into single-phase cubic LLZO. Rietveld refinement of the XRD pattern after calcination revealed the lattice parameter of the cubic Ga0.5-LLZO sample to be 12.977 Å; this value is in good agreement with those obtained in previous work for similar compositions [26, 56, 57].

The compositions of as-processed and calcined Ga0.5-LLZO powders were determined by ICP-OES

Table 2 Phase percentages and lattice parameters obtained from Rietveld analysis of undoped LLZO powder

| Fuel	Phases	Percentage (wt%)	Crystal system	Lattice Parameters (A)
As-processed: Undoped LLZO				
Urea	LLZO	80.9	Tetragonal	a = 13.128, c= 12.702
	$La_2Zr_2O_7$	12.4	Cubic	10.844
	La_2O_3	6.7	Hexagonal	a = 3.941,c = 6.134
Glycine	$La_2Zr_2O_7$	100.0	Cubic	10.939
Calcined (950 °C/5 h): Undoped LLZO				
Urea	LLZO	100.0	Tetragonal	a = 13.118, c = 12.682
Glycine	LLZO	68.9	Tetragonal	a = 12.996, c = 12.980
	$La_2Zr_2O_7$	21.0	Cubic	10.810
	La_2O_3	10.1	Hexagonal	a = 3.936, c = 6.127
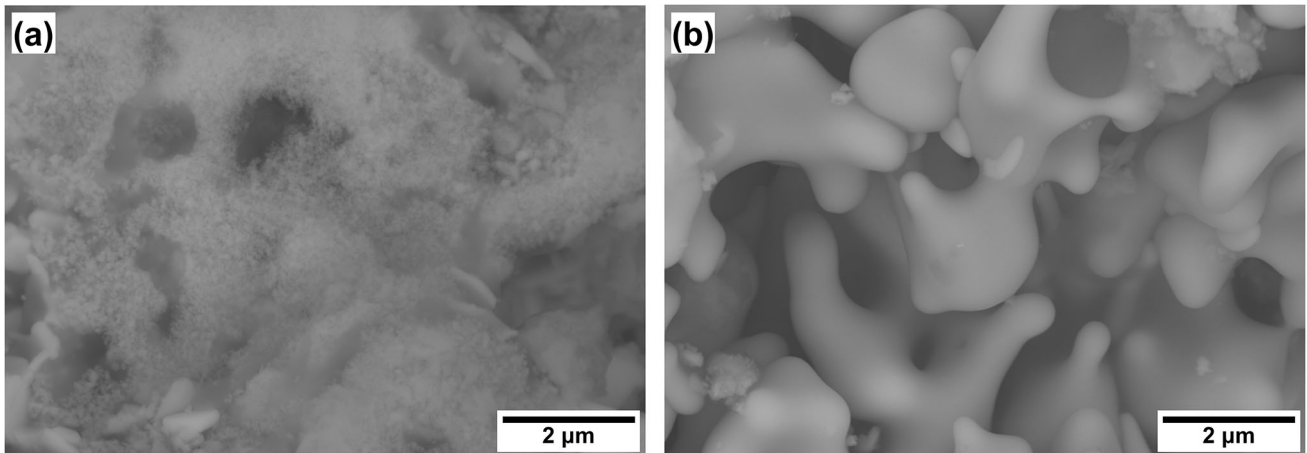
Figure 3 SEM images of (**a**) as-processed and (**b**) calcined (950 °C/5 h) undoped LLZO fabricated with urea as the fuel.

Figure 4 XRD patterns of as-processed and calcined Ga0.5-LLZO powder prepared via microwave-assisted SCS.
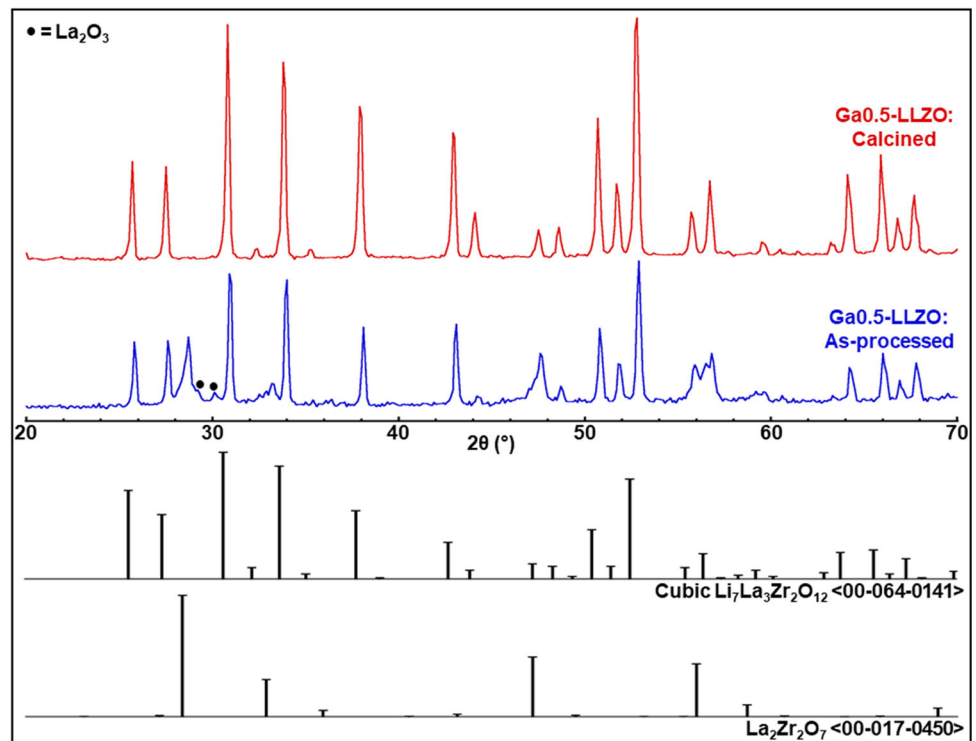
analysis. For the as-processed sample with a target Li:Ga:La:Zr cation ratio of 6.05:0.5:3:2 (i.e., with excess 10 mol% Li addition), the stoichiometry was calculated to be $Li_{6.46}Ga_{0.49}La_{3.00}Zr_{1.87}O_{12.20}$. While the measured Li content is approximately 6.8% higher than the targeted concentration, it is within the measurement uncertainty of ± 10 %. Furthermore, the ICP results obtained for as-processed Ga0.5-LLZO support a scenario whereby the rapid heating and cooling rates associated with the SCS method serve to

minimize Li loss. Upon calcination, the stoichiometry of the Ga0.5-LLZO powder was determined to be $Li_{5.45}Ga_{0.47}La_{3.00}Zr_{1.78}O_{11.55}$. Here, a difference of less than 1% is observed between the measured Li content and that in Ga0.5-LLZO with an ideal stoichiometry ($Li_{5.5}Ga_{0.5}La_3Zr_2O_{12}$). Interestingly, both the as-processed and calcined Ga0.5-LLZO samples show concentrations of Zr that are less than the ideal value. A similar finding of lower Zr contents has been observed in previous work, and the origin of this

result is currently not well understood [57]. Regardless, the results show a relative absence of Li loss after the SCS reaction and, due to the addition of a suitable content of excess Li, single-phase Ga0.5-LLZO powder is formed upon calcination. The development of optimized sintering protocols and ionic conductivity measurements of pellets obtained from the as-processed powders are reserved for future work. However, the obtained findings suggest that, with an optimized precursor formulation, it may be possible to fabricate single-phase Ga0.5-LLZO powder in a one-step microwave SCS reaction.

Conclusions

In this work, undoped and Ga-doped LLZO powders were successfully fabricated by microwave-assisted SCS. Two fuels, glycine and urea, were first utilized to synthesize undoped LLZO. In contrast to the trend in calculated T_{ad} values, the SCS reaction with urea reached much higher temperatures and was sustained over a longer duration. The reduced temperatures and incomplete combustion with glycine could be attributable to more thermodynamically stable metal-glycine complexes when compared to urea. Partial crystallization into tetragonal LLZO was achieved with urea from the heat released in the SCS reaction; subsequent calcination (950 °C/5 h) of the powder yielded single-phase tetragonal LLZO. With urea as the fuel, SCS reactions to produce Ga-doped LLZO were carried out; partial crystallization of the product into cubic LLZO was achieved after combustion and full crystallization into single phase cubic LLZO was attained after calcination. ICP analysis revealed a relative absence of Li loss for as-processed Ga-doped LLZO and a less than 1% difference between the measured and ideal Li contents for calcined Ga-doped LLZO powder. With further optimization of reaction chemistry and/or a mixture of different fuels, the synthesis of single-phase cubic LLZO via microwave-assisted SCS without the need for a crystallization heat treatment may be possible.

Acknowledgements

Declarations

Conflict of interest The authors declare that they have no conflicts of interest.

References

[1] Quartarone E, Mustarelli P (2020) Review—emerging trends in the design of electrolytes for lithium and post-lithium batteries. J Electrochem Soc 167:050508. https://doi.org/10.1149/1945-7111/ab63c4

[2] Roth EP, Orendorff CJ (2012) How electrolytes influence battery safety. Interface magazine 21:45–49. https://doi.org/10.1149/2.f04122if

[3] Tarascon J-M (2010) Key challenges in future Li-battery research. Phil Trans R Soc A 368:3227–3241. https://doi.org/10.1098/rsta.2010.0112

[4] Kil E-H, Choi K-H, Ha H-J, Xu S, Rogers JA, Kim MR, Lee Y-G, Kim KM, Cho KY, Lee S-Y (2013) Imprintable, bendable, and shape-conformable polymer electrolytes for versatile-shaped lithium-ion batteries. Adv Mater 25:1395–1400. https://doi.org/10.1002/adma.201204182

[5] Inaguma Y, Liquan C, Itoh M, Nakamura T, Uchida T, Ikuta H, Wakihara M (1993) High ionic conductivity in lithium lanthanum titanate. Solid State Comm 86:689–693. https://doi.org/10.1016/0038-1098(93)90841-A

[6] Kamaya N, Homma K, Yamakawa Y, Hirayama M, Kanno R, Yonemura M, Kamiyama T, Kato Y, Hama S, Kawamoto K, Mitsui A (2011) A lithium superionic conductor. Nat Mater 10:682–686. https://doi.org/10.1038/nmat3066

[7] Kim JM, Park GB, Lee KC, Park HY, Nam SC, Song SW (2009) Li–B–O–N electrolytes for all-solid-state thin film batteries. J Power Sources 189:211–216. https://doi.org/10.1016/j.jpowsour.2008.09.089

[8] Murugan R, Thangadurai V, Weppner W (2007) Fast lithium ion conduction in garnet-Type $Li_7La_3Zr_2O_{12}$. Angew Chem Int Ed 46:7778–7781. https://doi.org/10.1002/anie.200701144

[9] Yao X, Huang B, Yin J, Peng G, Huang Z, Gao C, Liu D, Xu X (2016) All-solid-state lithium batteries with inorganic solid electrolytes: Review of fundamental science. Chin Phys B 25:018802. https://doi.org/10.1088/1674-1056/25/1/018802

[10] Zhang Y, He X, Chen Z, Bai Q, Nolan AM, Roberts CA, Banerjee D, Matsunaga T, Mo Y, Ling C (2019) Unsupervised discovery of solid-state lithium ion conductors. Nature Comm 10:5260. https://doi.org/10.1038/s41467-019-13214-1

[11] Allen JL, Wolfenstine J, Rangasamy E, Sakamoto J (2012) Effect of substitution (Ta, Al, Ga) on the conductivity of $Li_7La_3Zr_2O_{12}$. J Power Sources 206:315–319. https://doi.org/10.1016/j.jpowsour.2012.01.131

[12] Illbeigi M, Fazlali A, Kazazi M, Mohammadi AH (2016) Effect of simultaneous addition of aluminum and chromium on the lithium ionic conductivity of $LiGe_2(PO_4)_3$ NASICON-type glass–ceramics. Solid State Ionics 289:180–187. https://doi.org/10.1016/j.ssi.2016.03.012

[13] Loho C, Djenadic R, Bruns M, Clemens O, Hahn H (2017) Garnet-type $Li_7La_3Zr_2O_{12}$ solid electrolyte thin films grown by CO_2-laser assisted CVD for all-solid-state batteries. J Electrochem Soc 164:A6131–A6139. https://doi.org/10.1149/2.0201701jes

[14] Manthiram A, Yu X, Wang S (2017) Lithium battery chemistries enabled by solid-state electrolytes. Nat Rev Mater 2:16103. https://doi.org/10.1038/natrevmats.2016.103

[15] Rawlence M, Filippin AN, Wäckerlin A, Lin TY, Cuervo-Reyes E, Remhof A, Battaglia C, Rupp JLM, Buecheler S (2018) Effect of gallium substitution on lithium-ion conductivity and phase evolution in sputtered $Li_{7-3x}Ga_xLa_3Zr_2O_{12}$ thin films. ACS Appl Mater Interfaces 10:13720–13728. https://doi.org/10.1021/acsami.8b03163

[16] Sastre J, Priebe A, Döbeli M, Michler J, Tiwari AN, Romanyuk YE (2020) Lithium garnet $Li_7La_3Zr_2O_{12}$ electrolyte for all-solid-state batteries: closing the gap between bulk and thin film li-ion conductivities. Adv Mater Interfaces 7:2000425. https://doi.org/10.1002/admi.202000425

[17] Rawlence M, Garbayo I, Buecheler S, Rupp JLM (2016) On the chemical stability of post-lithiated garnet Al-stabilized $Li_7La_3Zr_2O_{12}$ solid state electrolyte thin films. Nanoscale 8:14746–14753. https://doi.org/10.1039/C6NR04162K

[18] Samson AJ, Hofstetter K, Bag S, Thangadurai V (2019) A bird's-eye view of Li-stuffed garnet-type $Li_7La_3Zr_2O_{12}$ ceramic electrolytes for advanced all-solid-state Li batteries. Energy Environ Sci 12:2957–2975. https://doi.org/10.1039/C9EE01548E

[19] Thangadurai V, Pinzaru D, Narayanan S, Baral AK (2015) Fast solid-state Li ion conducting garnet-type structure metal oxides for energy storage. J Phys Chem Lett 6:292–299. https://doi.org/10.1021/jz501828v

[20] Thompson T, Yu S, Williams L, Schmidt RD, Garcia-Mendez R, Wolfenstine J, Allen JL, Kioupakis E, Siegel DJ, Sakamoto J (2017) Electrochemical window of the Li-ion solid electrolyte $Li_7La_3Zr_2O_{12}$. ACS Energy Lett 2:462–468. https://doi.org/10.1021/acsenergylett.6b00593

[21] Zhu Y, He X, Mo Y (2015) Origin of outstanding stability in the lithium solid electrolyte materials: insights from thermodynamic analyses based on first-principles calculations. ACS Appl Mater Interfaces 7:23685–23693. https://doi.org/10.1021/acsami.5b07517

[22] Teprovich JA Jr, Colon Mercado H, Olson L, Ganesan P, Babineau D, Garcia-Diaz BL (2019) Electrochemical extraction of hydrogen isotopes from Li/LiT mixtures. Fusion Eng Des 139:1–6. https://doi.org/10.1016/j.fusengdes.2018.11.018

[23] Bernstein N, Johannes MD, Hoang K (2012) Origin of the structural phase transition in $Li_7La_3Zr_2O_{12}$. Phys Rev Lett 109:205702. https://doi.org/10.1103/PhysRevLett.109.205702

[24] Geiger CA, Alekseev E, Lazic B, Fisch M, Armbruster T, Langner R, Fechtelkord M, Kim N, Pettke T, Weppner W (2011) Crystal chemistry and stability of "$Li_7La_3Zr_2O_{12}$" garnet: a fast lithium-ion conductor. Inorg Chem 50:1089–1097. https://doi.org/10.1021/ic101914e

[25] Rettenwander D, Blaha P, Laskowski R, Schwarz K, Bottke P, Wilkening M, Geiger CA, Amthauer G (2014) DFT study of the role of Al^{3+} in the fast ion-conductor $Li_{7-3x}Al_{3+x}La_3Zr_2O_{12}$ garnet. Chem Mater 26:2617–2623. https://doi.org/10.1021/cm5000999

[26] Li C, Liu Y, He J, Brinkman KS (2017) Ga-substituted $Li_7La_3Zr_2O_{12}$: An investigation based on grain coarsening in garnet-type lithium ion conductors. J Alloys Compd 695:3744–3752. https://doi.org/10.1016/j.jallcom.2016.11.277

[27] Wolfenstine J, Ratchford J, Rangasamy E, Sakamoto J, Allen JL (2012) Synthesis and high Li-ion conductivity of Ga-stabilized cubic $Li_7La_3Zr_2O_{12}$. Mater Chem Phys 134:571–575. https://doi.org/10.1016/j.matchemphys.2012.03.054

[28] Lan W, Fan H, Lau VW-h, Zhang J, Zhang J, Zhao R, Chen H, (2020) Realizing $Li_7La_3Zr_2O_{12}$ garnets with high Li^+ conductivity and dense microstructures by Ga/Nb dual substitution for lithium solid-state battery applications. Sustain Energy Fuels 4:1812–1821. https://doi.org/10.1039/C9SE01162E

[29] Li C, Ishii A, Roy L, Hitchcock D, Meng Y, Brinkman K (2020) Solid-state reactive sintering of dense and highly conductive Ta-doped $Li_7La_3Zr_2O_{12}$ using CuO as a sintering aid. J Mater Sci 55:16470–16481. https://doi.org/10.1007/s10853-020-05221-1

[30] Thompson T, Wolfenstine J, Allen JL, Johannes M, Huq A, David IN, Sakamoto J (2014) Tetragonal vs. cubic phase stability in Al-free Ta doped $Li_7La_3Zr_2O_{12}$ (LLZO). J Mater

Chem A 2:13431–13436. https://doi.org/10.1039/C4TA02099E

[31] Paolella A, Zhu W, Bertoni G, Savoie S, Feng Z, Demers H, Gariepy V, Girard G, Rivard E, Delaporte N, Guerfi A, Lorrmann H, George C, Zaghib K (2020) Discovering the influence of lithium loss on garnet $Li_7La_3Zr_2O_{12}$ electrolyte phase stability. ACS Appl Energy Mater 3:3415–3424. https://doi.org/10.1021/acsaem.9b02401

[32] Xue W, Yang Y, Yang Q, Liu Y, Wang L, Chen C, Cheng R (2018) The effect of sintering process on lithium ionic conductivity of $Li_{6.4}Al_{0.2}La_3Zr_2O_{12}$ garnet produced by solid-state synthesis. RSC Adv 8:13083–13088. https://doi.org/10.1039/C8RA01329B

[33] Jonson RA, McGinn PJ (2018) Tape casting and sintering of $Li_7La_3Zr_{1.75}Nb_{0.25}Al_{0.1}O_{12}$ with Li_3BO_3 additions. Solid State Ion 323:49–55. https://doi.org/10.1016/j.ssi.2018.05.015

[34] Jin Y, McGinn PJ (2011) Al-doped $Li_7La_3Zr_2O_{12}$ synthesized by a polymerized complex method. J Power Sources 196:8683–8687. https://doi.org/10.1016/j.jpowsour.2011.05.065

[35] Janani N, Ramakumar S, Dhivya L, Deviannapoorani C, Saranya K, Murugan R (2011) Synthesis of cubic $Li_7La_3Zr_2O_{12}$ by modified sol–gel process. Ionics 17:575–580. https://doi.org/10.1007/s11581-011-0611-x

[36] Badami P, Smetaczek S, Limbeck A, Rettenwander D, Chan CK, Kannan ANM (2021) Facile synthesis of Al-stabilized lithium garnets by a solution-combustion technique for all solid-state batteries. Mater Adv 2:5181–5188. https://doi.org/10.1039/D1MA00393C

[37] Dhivya L, Karthik K, Ramakumar S, Murugan R (2015) Facile synthesis of high lithium ion conductive cubic phase lithium garnets for electrochemical energy storage devices. RSC Adv 5:96042–96051. https://doi.org/10.1039/C5RA18543B

[38] Weller JM, Chan CK (2020) Reduction in Formation Temperature of Ta-Doped Lithium Lanthanum Zirconate by Application of Lux-Flood Basic Molten Salt Synthesis. ACS Appl Energy Mater 3:6466–6475. https://doi.org/10.1021/acsaem.0c00716

[39] Kun R, Langer F, Delle Piane M, Ohno S, Zeier WG, Gockeln M, Colombi Ciacchi L, Busse M, Fekete I (2018) Structural and computational assessment of the influence of wet-chemical post-processing of the Al-substituted cubic $Li_7La_3Zr_2O_{12}$. ACS Appl Mater Interfaces 10:37188–37197. https://doi.org/10.1021/acsami.8b09789

[40] Jain SR, Adiga KC, Verneker VRP (1981) A new approach to thermochemical calculations of condensed fuel-oxidizer mixtures. Combust Flame 40:71–79. https://doi.org/10.1016/0010-2180(81)90111-5

[41] Ishii A, Ishijima H, Kobayashi K, Oikawa I, Takamura H (2022) Insight into low-temperature sintering of samarium-doped ceria mixed with scavenging lithium. Acta Mater 224:117529. https://doi.org/10.1016/j.actamat.2021.117529

[42] Xia W, Xu B, Duan H, Guo Y, Kang H, Li H, Liu H (2016) Ionic conductivity and air stability of Al-Doped $Li_7La_3Zr_2O_{12}$ sintered in alumina and Pt crucibles. ACS Appl Mater Interfaces 8:5335–5342. https://doi.org/10.1021/acsami.5b12186

[43] Varma A, Mukasyan AS, Rogachev AS, Manukyan KV (2016) Solution combustion synthesis of nanoscale materials. Chem Rev 116:14493–14586. https://doi.org/10.1021/acs.chemrev.6b00279

[44] Dean JA (1999) Lange's handbook of chemistry, 15th edn. McGraw-Hill, New York

[45] Harl RR (2013) Processing considerations of the combustion synthesis of yttrium aluminum garnet powders. Ph.D. dissertation, Vanderbilt University.

[46] Il'ina EA, Raskovalov AA, Reznitskikh OG (2019) Thermodynamic properties of solid electrolyte $Li_7La_3Zr_2O_{12}$. J Chem Thermodyn 128:68–73. https://doi.org/10.1016/j.jct.2018.08.009

[47] Smith JM, Van Ness HC, Abbott MM, Swihart MT (2018) Introduction to chemical engineering thermodynamics, 8th edn. McGraw-Hill, New York

[48] Zhuravlev VD, Bamburov VG, Beketov AR, Perelyaeva LA, Baklanova IV, Sivtsova OV, Vasil'ev VG, Vladimirova EV, Shevchenko VG, Grigorov IG (2013) Solution combustion synthesis of alpha-Al_2O_3 using urea. Ceram Int 39:1379–1384. https://doi.org/10.1016/j.ceramint.2012.07.078

[49] Fumo DA, Morelli MR, Segadaes AM (1996) Combustion synthesis of calcium aluminates. Mater Res Bull 31:1243–1255

[50] Mukasyan AS (2011) Solution combustion as a promising method for the synthesis of nanomaterials. Adv Sci Tech 63:187–196. https://doi.org/10.4028/www.scientific.net/AST.63.187

[51] Mukasyan AS, Dinka P (2007) Novel approaches to solution-combustion synthesis of nanomaterials. Int J Self-Propagating High-Temp Synth 16:23–35. https://doi.org/10.3103/s1061386207010049

[52] Purohit RD, Sharma BP, Pillai KT, Tyagi AK (2001) Ultrafine ceria powders via glycine-nitrate combustion. Mater Res Bull 36:2711–2721. https://doi.org/10.1016/S0025-5408(01)00762-0

[53] da Conceicao L, Silva AM, Ribeiro NFP, Souza M (2011) Combustion synthesis of $La_{0.7}Sr_{0.3}Co_{0.5}Fe_{0.5}O_3$ (LSCF) porous materials for application as cathode in IT-SOFC.

Mater Res Bull 46:308–314. https://doi.org/10.1016/j.materresbull.2010.10.009

[54] Megahed AS, Ibrahim O, Adam A, Al Majthoub Md (2014) Complexes of urea with aluminum (III) chloride and acetate. Int J Chem Sci 12:429–437

[55] Murphy JM, Powell BA, Brumaghim JL (2020) Stability constants of bio-relevant, redox-active metals with amino acids: The challenges of weakly binding ligands. Coord Chem Rev 412:213253. https://doi.org/10.1016/j.ccr.2020.213253

[56] Afyon S, Krumeich F, Rupp JLM (2015) A shortcut to garnet-type fast Li-ion conductors for all-solid state batteries. J Mater Chem A 3:18636–18648. https://doi.org/10.1039/C5TA03239C

[57] Birkner N, Li C, Estes SL, Brinkman KS (2021) Gallium-doping effects on structure, lithium-conduction, and thermochemical stability of $Li_{7-3x}Ga_xLa_3Zr_2O_{12}$ garnet-type electrolytes. Chemsuschem 14:2621–2630. https://doi.org/10.1002/cssc.202100526